Biodegradable Core/Shell Fibers by Coaxial Electrospinning: Processing, Fiber Characterization, and Its Application in Sustained Drug Release

4 AUTHORS, INCLUDING:

Chi Wang
National Cheng Kung University
69 PUBLICATIONS **1,189** CITATIONS

SEE PROFILE

Yi-Dong Lin
Harvard Medical School
9 PUBLICATIONS **152** CITATIONS

SEE PROFILE

Macromolecules
ARTICLE

Biodegradable Core/Shell Fibers by Coaxial Electrospinning: Processing, Fiber Characterization, and Its Application in Sustained Drug Release

Chi Wang,*,[†] Kuo-Wei Yan,[†] Yi-Dong Lin,[‡] and Patrick C. H. Hsieh[‡]

[†]*Department of Chemical Engineering, National Cheng Kung University, Tainan 701, Taiwan, and*
[‡]*Institute of Clinical Medicine, Department of Surgery, and Institute of Biomedical Engineering, National Cheng Kung University, Tainan 701, Taiwan*

Received February 23, 2010; Revised Manuscript Received June 21, 2010

ABSTRACT: Solutions of two biodegradable polymers, that is, poly(DL-lactic acid) (PDLLA) and poly-(3-hydroxy butyrate) (PHB), were individually delivered to the inner and outer channel of a coaxial-tube spinneret for electrospinning to prepare core−shell fibers used for drug release applications. By interchanging the inner- and outer-channel solutions, either PDLLA/PHB or PHB/PDLLA core−shell fibers could be conveniently obtained. Their fiber diameters were readily controlled by the flow rate of the core fluid (Q_c). The effects of Q_c on the morphologies of the Taylor cone, the whipping jet, and the electrospun fibers were investigated. Several scaling laws describing the Q_c dependence of the outer fiber diameter (D_f) and the inner fiber diameter (d_f) were derived, that is, $D_f \sim Q_c^{0.02}$ and $d_f \sim Q_c^{0.18}$ for the PDLLA/PHB fluids and $D_f \sim Q_c^{0.30}$ and $d_f \sim Q_c^{0.59}$ for the PHB/PDLLA fluids. These scaling laws provided the processing guidelines for the manipulation of the final diameters of the core−shell fibers for a given pair of electrospinning solutions. The microstructure revealed by differential scanning calorimetry, Fourier transform infrared spectroscopy, and wide-angle X-ray diffraction showed that the PDLLA component was in the amorphous state. In addition, the crystallizability of the PHB component remained relatively unchanged despite the reduction of its measured melting enthalpy when the PDLLA content was increased through an increase in its flow rate. By controlling Q_c, PDLLA/PHB fibers with a PHB shell of a similar crystallinity but with different thicknesses were readily obtained and used for the sustained release of dimethyloxalylglycine (DMOG) drug, which is a proangiogenic compound acting via the hypoxia-inducible factor system. In contrast with the single-component PDLLA and PHB fibers, which exhibited a burst release behavior, two-stage release kinetics was observed for the present PDLLA/PHB fibers when DMOG was embedded in the core section: an initial fast release before the inflections followed by a constant release. For the first stage, the amount released was ∼25% within 60 h, irrespective of the PHB thickness. After the burst release, DMOG was linearly released up to an amount of 70%, and the release rate was feasibly controlled by the thickness of the PHB shell.

Introduction

Electrospinning is a promising technique for the production of polymeric fibers with diameters ranging from micro- to nanometer scale, depending on the solution properties (e.g., viscosity, conductivity, and surface tension) and processing variables (e.g., flow rate, applied voltage, and working distance). Extensive studies have been performed using the single-tube spinneret to prepare many varieties of single-component nanofibers.[1−4] Using a coaxial-tube spinneret with two different solutions, which are pumped to the inner tube and outer tube, electrospun fibers with core−shell structures can be fabricated.[5−13] In contrast with the single-component fibers, core−shell fibers provide a feasible route for a better controlled release of embedded chemicals and drugs[14−20] through an adjustment of the fiber microstructure (e.g., crystallinity, crystal orientation, and crystal dimension) as well as the fiber diameters. To yield the fiber structure successfully, a sufficient entanglement density in the electrospinning solution is generally required.[21,22] In other words, a minimum viscosity is required for a given polymer/solvent pair to maintain the solution in an entangled regime. It has been demonstrated that viscosity is an important solution property in determining the fiber diameter;[21] the lower the solution viscosity, the thinner the fibers are.

*Corresponding author: Tel +886-6-2757575 ext. 62645; Fax +886-6-2344496; e-mail chiwang@mail.ncku.edu.tw.

Recently, much attention has been given to the development of biomaterials, such as ploy(lactic acid) (PLA) and poly[(R)-3-hydroxy butyrate] (PHB), because of their environmentally friendly properties. Of significant importance are their applications as tissue scaffolds owing to their specific biocompatible and biodegradable behaviors. PHB is known to be a semicrystalline polymer with a brittle fracture behavior, whereas PLA can be either semicrystalline or amorphous depending on the relative ratio of its PLA backbone chain D-form/L-form, which is designed through chemical syntheses. Because of their large surface area per unit volume, electrospun PHB and PLA fiber membranes have received widespread interest in the application of cell culture. In spite of the intensive studies on electrospun single-component PHB[23−25] and PLA[26−31] fibers, the fabrication of core−shell fibers based on these two key constituents has not yet been reported. In fact, most of the current research focused on the application aspect, and only a few articles[9,12,18] discussed the influence of the processing variables on the diameter of the core−shell fibers. Using solutions of poly(ethylene glycol) (PEG) and poly(ε-caprolactone), Ramakrishna's group[18] found that the outer fiber diameter increases with the core fluid flow rate (Q_c), provided that the shell fluid flow rate (Q_s) is fixed. Rutledge's group[9] prepared silk/poly(ethylene oxide) core−shell fibers with different diameters by changing the Q_c and Q_s. They concluded that the outer fiber diameter increases with Q_s but is

relatively independent of Q_c, whereas the inner fiber diameter increases with Q_c. On the basis of their results, Q_c can be considered a convenient parameter for preparing core−shell fibers with a constant outer diameter and a variable inner diameter: an ideal model for understanding the chemical release mechanism in the core−shell fiber system.

This study aims to manipulate the electrified jet with controlled properties to obtain the desired fiber diameter and to gain a complete understanding of the Q_c effects on the morphologies of the cone/jet/fiber developed during coaxial electrospinning of the amorphous poly(DL-lactic acid) (PDLLA) and crystallizable PHB solutions. A three-tube spinneret was designed and constructed. The solvent vapor of the shell fluid was introduced by the outmost gas jacket for coaxial electrospinning in an attempt to reduce moisture attack, which frequently results in the clogging of the Taylor cone. By interchanging both solutions to the inner and outer tube of the spinneret, alternative core−shell fibers of PDLLA/PHB and PHB/PDLLA could be obtained. To our knowledge, there has been no report addressing the issue of fluid exchange on the coaxial electrospinning process. Our results presented a relation between Q_c and the electrospun products, by which the inner and outer diameter of the core−shell fibers could be predicted. The microstructure of as-spun fibers was characterized by several analytical techniques. A detailed study, starting from the properties of electrospinning solutions to the internal structure of the electrospun fibers, was presented. Finally, the release of drugs from the as-spun core−shell fibers was investigated using dimethyloxalylglycine (DMOG) as the model drug. Frequently used as a proangiogenic compound, DMOG acts via the HIF-1 system.[32,33] By carefully controlling the microstructure and shell diameter, two-stage release kinetics with controllable release rates was achieved in the present study.

Experimental Section

Solution Preparation and Properties. PDLLA pellets and PHB powder samples were purchased from Natureworks LLC and Sigma-Aldrich, respectively. DMOG (catalog no. EI-347-0010) was purchased from Enzo Life Sciences, Inc. The molar content of D-lactide units in the PDLLA was estimated to be 10% using a JASCO DIP-370 polarimeter at a wavelength of 589 nm. Using gel permeation chromatography (GPC) with chloroform (CF) as the mobile phase, the measured weight-average molecular weight (M_w) and polydispersity index of PDLLA were determined to be 1.78×10^5 g/mol and 2.1, respectively. Using an Ubbelohde capillary viscometer, the intrinsic viscosity, $[\eta]$, of the PHB in CF was determined to be 2.136 dL/g, which gave an average molecular weight of 2.62×10^5 g/mol based on the Mark−Houwink−Sakurada equation with the reported values of $K (= 7.7 \times 10^{-5})$ and $a (= 0.82)$.[34] The intrinsic viscosity of PDLLA in dimethylformamide (DMF) was also measured to be 0.9825 dL/g. The electrospinning solutions were prepared with different PDLLA concentrations in DMF. To prepare the PHB solution, a cosolvent of CF and DMF was used with a weight ratio of 9/1. The reported solubility parameters for PDLLA, PHB, CF, and DMF were 10.6−11.4, 9.7, 9.3, and 12.1 (cal/cm³)^0.5, respectively. Solutions were prepared on a weight basis, and the volume fraction of polymer (ϕ_v) was calculated from the pure component densities ($\rho_{CF} = 1.480$, $\rho_{DMF} = 0.944$, $\rho_{PDLLA} = 1.230$, and $\rho_{PHB} = 1.230$ g/cm³), assuming negligible volume change on mixing. Solution properties, such as surface tension (γ), conductivity (κ), and zero shear viscosity (η_0), were measured using the Face surface tension meter (CBVP-A3), Consort conductivity meter (C832), and Brookfield viscometer (LVDV-I+, spindle 18, and cup 13R), respectively.

Electrospinning and Measurements. Figure 1a shows the coaxial-tube spinneret used to prepare the core−shell fibers. The outer diameters of the three-tube spinnerets were 0.81, 1.68, and 6.10 mm. The outermost tube was used as a gas jacket for reducing the solvent evaporation rate when the solvent vapor of
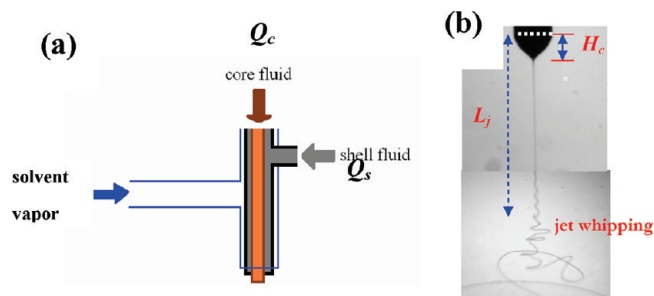

Figure 1. (a) Three-tube spinneret used to prepare core/shell fibers; the flow rates of inner and outer fluids are Q_c and Q_s, respectively, and vapor of outer fluid solvent is introduced by N_2 carrier gas to encapsulate the Taylor cone to reduce the evaporation rate. The outer diameters of the inner tube, outer tube, and gas jacket are 0.81, 1.68, and 6.1 mm, respectively. (b) Stable cone−jet electrospinning mode showing the cone height, H_c, and the distance from the needle end, L_j, at where jet whipping starts to occur. The dotted line represents the needle end. The cone morphology is obtained by a conventional CCD, whereas the jet whipping morphology is obtained by a high-speed camera with a frame rate of 2000 frames/s.

the shell fluid was introduced to encapsulate the Taylor cone. N_2 was used as the carrier gas, and the flow rate was controlled in a range of 50−100 mL/min for not interrupting the whipping jet.[31] To obtain PDLLA/PHB core−shell fibers, the prepared PDLLA and PHB solutions were separately delivered by two syringe pumps (Cole-Parmer) to the inner and outer tube with controlled flow rates of Q_c and Q_s, respectively. By exchanging the core−shell fluids, PHB/PDLLA core−shell fibers were readily obtained instead. A high electrical voltage (V) was applied to the spinneret by a high-voltage source (Bertan, 205B) to provide a sufficient electric field for electrospinning. To construct a needle-to-plate electrode configuration, a steel net (30×30 cm²) was used as a collector for the electrospun fibers at a certain working distance (H) below the spinneret tip. Although H shows a negligible influence on the diameter of electrospun fibers,[25] a minimum H is generally required for solvent evaporation to prepare solvent-free fibers. Thus, H was fixed at 28 cm for this purpose. During electrospinning, the morphologies of the electrified cone and jet were monitored to derive the following: (i) the cone height, H_c, which is defined as the distance from the spinneret end to the Taylor cone apex; (ii) the length of straight jet, l_j, which is measured from the apex of the Taylor cone to the initiation of jet whipping; and (iii) the terminal jet diameter at the end of the straight jet, D_j, which was determined by a laser diffraction technique. The jet whipping behavior was observed by a high-speed camera (Redlake, Motion Pro 10000). The length from the needle end to the initial jet whipping was denoted as L_j ($= H_c + l_j$). The morphology of the stable cone−jet electrospinning mode is shown in Figure 1b. The experimental details are described in a previous article.[25] It has been pointed out that the final fiber diameter is relevant with the jet diameter as well as how effectively the jet whipping takes place.[31] For the present needle-to-plate configuration setup, the electric field strength was highly nonuniform and concentrated around the needle end. As the electric field decays exponentially with the distance from the needle end,[25] a larger L_j eventually led to a lower field strength for jet whipping, which in turn produced fatter fibers.

Fiber Characterization. The morphology of the fibers was observed under a scanning electron microscope (SEM, Hitachi S4100), and the average fiber diameter (d_f) was measured from a collection of ∼500 fibers diameters. Thermograms were obtained using a differential scanning calorimeter (DSC, Perkin-Elmer, DSC7) under a nitrogen atmosphere at a scanning rate of 20 °C/min. Crystallinity values were determined using the ratio of $\Delta H_f / \Delta H°_f$, where ΔH_f and $\Delta H°_f$ are the measured DSC heat of fusion and the heat of fusion for a 100% crystal, respectively. The $\Delta H°_f$ values of 93.1 and 146 J/g were used for the PLA[35] and PHB[36] components, respectively. The infrared spectra of the

fiber mats were obtained using a Fourier transform infrared (FTIR) spectrometer (Perkin-Elmer, 100) with a resolution of $2\,cm^{-1}$ and 64 scans. An X-ray generator (Rigaku, DMAX2000) with a Cu Kα beam was used to obtain the wide-angle X-ray diffraction (WAXD) intensity profile of the samples.

Drug Release Study. According to the manufacturer, DMF is miscible with DMOG. Our preliminary test showed that DMOG could also be dissolved in chloroform. The DMOG drug was incorporated into the polymer solution prior to electrospinning at a given loading per polymer weight. After electrospinning, the fiber mats were cut into $1.5 \times 1.5\,cm^2$ sections, and each section was incubated at 37 °C in 100 mL of PBS buffer solution (pH = 7.4). The DMOG release from the electrospun fibers was monitored by a UV−vis spectrophotometer (Hitachi, U-2900) at a wavelength of 204 nm. At predetermined time intervals, 1 mL of the buffer was taken out to quantify the drug concentration. The UV absorbance of DMOG in the buffer was detected and converted to the drug concentration through a calibration curve of DMOG in the same buffer. In this manner, the cumulative amount of the released DMOG, based on the calculated amount in the samples from the feed composition, was calculated as a function of incubation time. Three membrane pieces of each kind were evaluated, and the average of cumulative released amounts was recorded.

Results and Discussion

In general, electrospun products with fiberlike structure can be obtained under the condition that a chain network is developed in the given electrospinning solution. For solutions with a concentration lower than the entanglement concentration (c_e), electrospinning is eventually degenerated to electrsopraying, which yields spherical particulates due to the capillary instability at the end of the straight jet. Thus, for a given polymer/solvent pair, the determination of c_e is an important task prior to electrospinning. Based on the method proposed by McKee et al.,[21] the log−log plot of the solution specific viscosity versus the volume fraction was constructed to obtain the c_e for the present PDLLA and PHB solutions, and the determined values were 10 and 5 wt %, respectively.[25,31] However, the terminal slope was different from each other. It was 4.68 for the PDLLA/DMF and 3.60 for the PHB/(CF/DMF) solution, which suggested the difference in the interaction of the polymer chain/solvent in the solution state. To yield bead-free fibers, our previous studies showed that a minimum concentration was required: 19 wt % for the PDLLA solution[31] and 7 wt % for the PHB solution.[25] On the basis of these findings, we chose the 20 wt % PDLLA solution and 7 wt % PHB solution as the core−shell fluids for the present study to prepare uniform electrospun fibers. The zero shear viscosity, conductivity, and surface tension of the selected PDLLA solution were measured to be 3780 cP, 3.74 µS/cm, and 37.5 dyn/cm, respectively. For the PHB solution, the corresponding values of η_0, κ, and γ were 319 cP, 2.45 µS/cm, and 28.8 dyn/cm. The PDLLA solution possessed a slightly higher conductivity and surface tension but a significantly larger viscosity than the PHB solution. By simply introducing the PDLLA solution into the inner tube in the absence of a shell fluid (Figure 1a), neat PDLLA fibers were readily obtained with a fiber diameter of 356 ± 89 nm. Similarly, neat PHB fibers with a diameter of 1.96 ± 0.31 µm were collected when the PHB solution was pumped to the outer tube in the absence of a core fluid. Remarkably, the electrospun PDLLA fibers possessed a lower diameter than the PHB fibers, although its solution viscosity was an order larger than that of the PHB solution. This striking difference was attributed to a lower L_j of the electrified PDLLA jet,[31] which experienced a more significant whipping process under a higher electric field to render further jet stretching prior to the solvent evaporation.

PDLLA/PHB Core/Shell Fibers. Electrospun fibers with the PDLLA component as the core and the PHB component as the shell section were readily obtained by introducing the
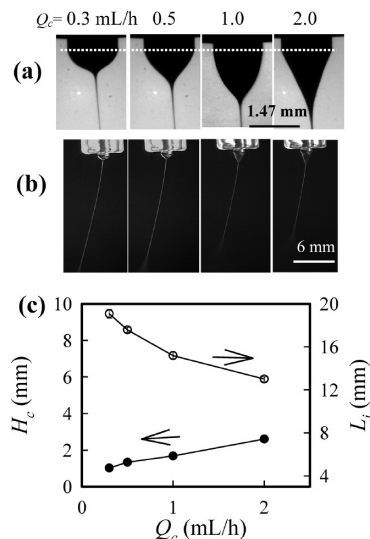

Figure 2. Q_c dependence of (a) cone morphology, (b) jet morphology, and (c) the measured H_c and L_j [PDLLA/PHB core/shell, $H = 28$ cm, $Q_s = 1.5$ mL/h, 10.5 kV].
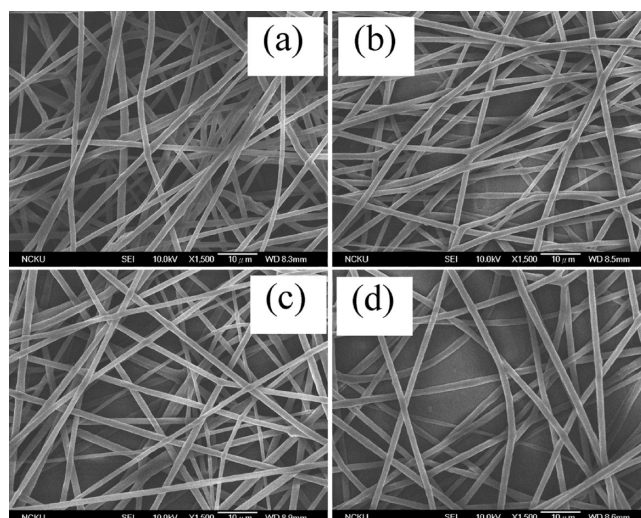

Figure 3. SEM images of PDLLA/PHB core/shell fibers obtained from different Q_c: (a) 0.3, (b) 0.5, (c) 1.0, and (d) 2.0 mL/h.

former solution to the inner tube and the latter solution to the outer tube. For a given Q_s of 1.5 mL/h, the processing window of V versus Q_c was first constructed to develop a stable cone−jet electrospinning mode (Figure S1).[37,38] Similar with the case of single-tube electrospinning,[25] a higher V was required for a larger Q_c. At a fixed Q_c, the range of applied V was rather small, and difficulties were encountered by varying V as an effective processing variable to control the fiber diameter. In contrast, the diameter of electrospun fibers can be conveniently manipulated by controlling the Q_c.[9,12,18] Based on the processing window, the Q_c available for the stable coaxial electrospinning was between 0.3 and 2.0 mL/h at a given V of 10.5 kV. Figure 2 shows the effect of Q_c on the morphologies of the Taylor cone and electrified jet. As the Q_c increased, the Taylor cone became bigger, but the straight jet length was reduced. The laser diffraction patterns of the straight jet end showed that the jet diameter (D_j) increased from 5.61 to 8.88 µm as the Q_c increased from 0.3 to 2.0 mL/h. Because of a thicker D_j, the electrospun fibers would be expected to be fatter when a larger Q_c is used. Shown in Figure 3 is the morphology of the as-spun core−shell fibers.
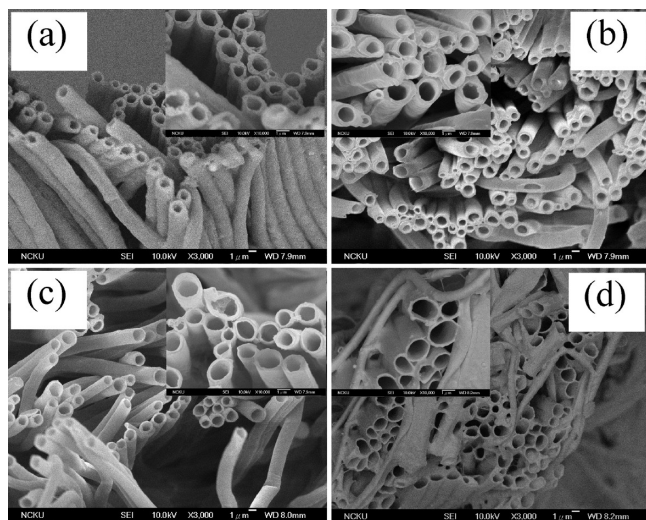
Figure 4. SEM images of PDLLA/PHB core/shell fibers after extracting the PDLLA core component using DMF. The electrospun fibers are obtained from different Q_c: (a) 0.3, (b) 0.5, (c) 1.0, and (d) 2.0 mL/h. The insets are higher magnification.

It should be noted that the outer fiber diameter (D_f) remained relatively unchanged at $\sim$1.50 μm despite a 7-fold difference in the applied Q_c. It has been demonstrated that for the electrospinning of a single-component solution a straight jet with a smaller jet diameter and shorter length can experience enhanced electric field for a more effective whipping process, leading to the production of fibers with a lower diameter.[31] Thus, the unexpected small value of D_f obtained from a large applied Q_c is attributed to the possession of a shorter straight jet (a smaller L_j, Figure 2), which experienced a more significant electric field for the jet whipping process. To reveal the inner fiber diameter (d_f), the as-spun core−shell fibers were cut first and then rinsed in excess amounts of DMF solvent to extract the PDLLA core component, leaving the PHB shell for SEM observations. The resulting morphology is shown in Figure 4, in which the hollow PHB fibers are evidently seen, and the corresponding d_f values are directly measured.

It was found that d_f increased with Q_c, although D_f exhibited a Q_c-independent trend. Thus, by carefully controlling the Q_c core−shell fibers with a fixed outer fiber diameter and variable shell thicknesses were readily produced for the drug release application (discussed in a later section). To verify further the d_f value, an indirect method was also used. Provided that D_f was obtained, the value of d_f could be estimated by eq 1 based on the assumption of equal stretching of the PDLLA and PHB solutions during the jet whipping process, which is valid for the elongational flow.

$$d_f = D_f[\phi'_v/(1+\phi'_v)]^{1/2} \quad (1)$$

where ϕ'_v is the volume ratio of the core−shell component (V_c/V_s). Two methods were applied to determine the corresponding ϕ'_v of the core−shell fibers: FTIR and flow-rate analyses.

The typical FTIR spectrum of an as-spun fiber membrane is shown by curve a in Figure 5a, where a pronounced curvature of the baseline at the high wavenumber region is observed due mainly to the noneven thickness of samples. Additional scattering and reflections associated with the voids in the fiber membranes even worsen the spectral quantity for precise analysis. The presence of a downward-pointing feature near the desirable wavenumber region of
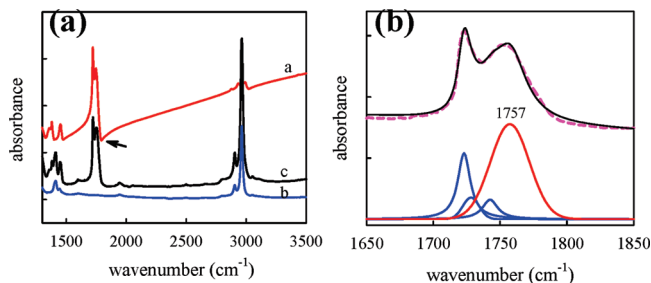

Figure 5. (a) FTIR spectra of a typical as-spun core/shell fiber membrane (curve a), PDMS fluid (curve b), and fiber membrane filled with PDMS fluid (curve c). The arrow shows the presence of an absorption dent. (b). FTIR spectra of PDLLA/PHB fibers obtained from electrospinning of solutions with Q_c = 1.0 mL/h and Q_s = 1.5 mL/h. The solid line and dashed line of the upper curves are the measured data and convolution of the individual bands (bottom curves). The band at 1757 cm^{-1} is related to the PDLLA, whereas the bands at 1742, 1728, and 1722 cm^{-1} are associated with the PHB chains in the amorphous, interfacial, and crystalline region, respectively.

carbonyl group (1650−1850 cm^{-1}) is important to note. This feature is attributed to the coupling of the real and imaginary parts of the refractive index caused by scattering, which results in a slightly dispersive line shape. To resolve this problem for a better quantitative analysis, several liquids were used to immerse the as-spun membrane to fill completely the porous space between fibers in an attempt to reduce abnormal scattering. The selected liquid was considered based on the following three requirements: (i) its surface tension has to be low enough to penetrate easily into the pore sites; (ii) it must be inert with respect to the fibers; and, more importantly, (iii) there should be no absorption resulting from the immersing fluid in the region of interest. Polydimethylsiloxane (PDMS) was found to be a suitable candidate to meet these characteristics. As shown in Figure 5a, the FTIR spectrum of the PDMS-wetted membrane (curve c) exhibits an even baseline, and the absorbance dent at 1790 cm^{-1} disappears. In addition, judging from the spectrum of the PDMS liquid (curve b), the absorbance in the range of 1650−1850 cm^{-1} was exclusively contributed by the carbonyl groups of PHB and PDLLA in the electrospun core−shell fibers. Using PDMS as the wetting medium, a precise determination of PDLLA/PHB amount in the core−shell fiber could be achieved by analyzing the FTIR spectra. Figure 5b shows a typical FTIR spectrum (range: 1650−1850 cm^{-1}) of the electrospun PDLLA/PHB fibers obtained under a given Q_c of 1.0 mL/h. The characteristic wavelength of the carbonyl group was 1757 cm^{-1} for the amorphous PDLLA,[40] whereas the bands at 1722, 1728, and 1742 cm^{-1} were attributed to the crystalline, interfacial, and amorphous phases of the PHB component, respectively.[41] Following the previous model analysis,[41] the deconvolution of the obtained spectrum was successfully performed to separate the contribution of both PDLLA and PHB components (bottom curves), from which the ratio of the carbonyl group content, X', of the as-spun core−shell fibers was derived. As each PDLLA and PHB monomer contains one carbonyl group, the volume ratio of ϕ'_v can be further derived after obtaining the value X'. Thus, eq 1 can be revised to

$$d_f = D_f[X'M'_0/(\rho'+X'M'_0)]^{1/2} \quad (2)$$

where M'_0 and ρ' are the monomer weight ratio and the solid density ratio of the core to shell components, respectively. Similarly, the ϕ'_v value of the electrospun fibers can be estimated by the predetermined flow-rate ratio of Q'
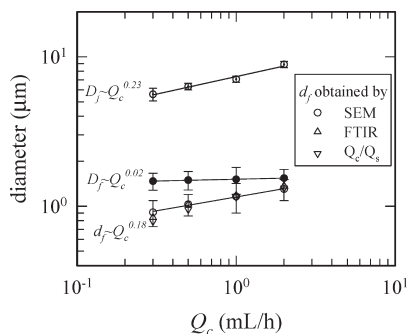
Figure 6. Q_c dependence of the jet diameter (D_j, ⊙), outer fiber diameter (D_f, ●), and inner fiber diameter (d_f: measured by (○) SEM, (△) FTIR, and (▽) flow rates) [Q_s = 1.5 mL/h, 10.5 kV, H = 28 cm].
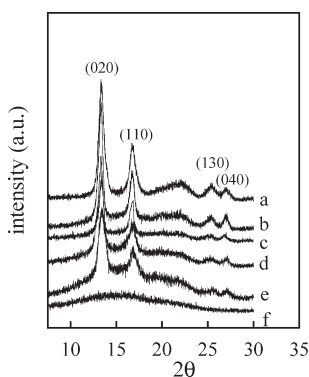

Figure 7. WAXD intensity profiles of the as-spun fibers. Single-component PHB and PDLLA fibers are represented by the curves a and f, respectively. The diffraction planes associated with the helical α crystalline form of PHB component are indexed. PDLLA/PHB core/shell fibers prepared by using different Q_c are shown by the curves (b) 0.3, (c) 0.5, (d) 1.0, and (e) 2.0 mL/h.

($= Q_c/Q_s$). Equation 1 can then be expressed by eq 3 as well.

$$d_f = D_f[Q'\rho_s'\phi_w'/(\rho'+Q'\rho_s'\phi_w')]^{1/2} \quad (3)$$

where ρ_s' and ϕ_w' are the density ratio and the weight fraction ratio of the core−shell solutions used for electrospinning, respectively. Figure 6 shows the Q_c dependence of d_f obtained directly from SEM and derived indirectly from FTIR results as well as the flow-rate ratio. Consistent data were obtained based on these tests, suggesting the valid assumption of equal stretching of the inner and outer jet. In other words, eqs 2 and 3 provided a fair guidance for the estimation of the inner fiber diameter without using the complicated fluorescence dye technique, which is generally applied to the core−shell fibers with a diameter of several micrometers. The Q_c dependence of d_f exhibited a power law relation, which could be expressed by $d_f \sim Q_c^{0.18}$. Given also in Figure 6 are the Q_c dependence of D_j and D_f, from which two additional scaling laws were derived as $D_j \sim Q_c^{0.23}$ and $D_f \sim Q_c^{0.02}$. The values of D_f were independent of the applied Q_c, and the exponent for the $D_j−Q_c$ relation was lower than that derived from the electrospinning of single-component solutions ($\sim$0.44−0.66).[31]

The WAXD profiles of the collected fibers electrospun from various Q_c are shown in Figure 7, together with that of the neat PHB fiber (curve a) and that of the neat PDLLA fiber (curve f). Accordingly, the single-component PDLLA fiber was amorphous, whereas the single-component PHB fibers possessed an orthorhombic α-form crystal with a
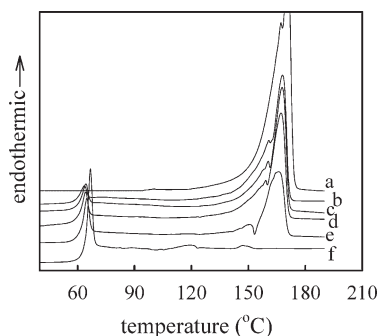

Figure 8. DSC heating traces of the as-spun fibers. Single-component PHB and PDLLA fibers are represented by the curves a and f, respectively. PDLLA/PHB core/shell fibers prepared by using different Q_c are shown by the curves (b) 0.3, (c) 0.5, (d) 1.0, and (e) 2.0 mL/h.

Table 1. Flow-Rate Effects on the Thermal Properties of As-Spun PDLLA/PHB Core/Shell Fibers[a]

Q_c (mL/h)	ϕ_{PHB} (wt)	$T_{g,PDLLA}$ (°C)	$\Delta H_r/\phi_{PDLLA}$ (J/g)	$T_{m,PHB}$ (°C)	ϕ^{DSC}/ϕ_{PHB}
0.3	0.62	58.1	3.43	160.7/168.0	0.57
0.5	0.52	58.9	3.43	160.1/167.8	0.62
1.0	0.41	59.0	3.91	158.8/167.2	0.65
2.0	0.29	59.5	4.91	149.4/166.0	0.63

[a] ϕ_{PHB} is the weight fraction of PHB component, which is determined from the ratio of $1 − (d_f/D_f)^2$ assuming both the density of PDLLA and PHB are the same at 1.23 g/cm³ [Q_s = 1.5 mL/h, 10.5 kV, H = 28 cm].

helical chain conformation. For the core−shell fibers, only diffraction peaks associated with the PHB component were observed in the absence of any discernible ones relevant to the PDLLA component, indicating that the PDLLA chains in the core section were also in the amorphous state. Judging from the broad diffraction peaks, the lateral size of α-form crystals developed in the PHB shell is reduced as the Q_c is increased. The DSC heating scans of the as-spun core−shell fibers fabricated at a rate of 20 °C/min are shown in Figure 8 as well as the heating traces of single-component PHB and PDLLA fibers. The neat PDLLA fibers were characterized by a stepwise increase in specific heat at the glass transition of 61.8 °C, followed by a distinctive enthalpy recovery endotherm (ΔH_r = 5.94 J/g). Another important feature of the thermal scans was the appearance of a cold crystallization peak at 95.6 °C, followed by two melting peaks at 119.7 and 146.7 °C. The measured enthalpy from both endotherms was 1.65 J/g, corresponding to a small crystallinity fraction of 0.018. On the basis of our previous study,[31] these unique features were attributed to the occurrence of phase separation during electrospinning, which yielded more trans−trans conforms. With more extended chain structures, the as-spun amorphous PDLLA fibers were in a position to undergo cold crystallization readily, which was not likely to occur in the usual circumstance during DSC heating. For the neat PHB fibers, no cold crystallization took place. Aside from the main melting peak at 170.8 °C, a small melting shoulder at 167.0 °C was observed, and the calculated crystallinity fraction, ϕ^{DSC}, was 0.61. For the core−shell fibers, the measured thermal properties are listed in Table 1 for comparison as well as the volume fraction of PHB component in the as-spun fibers (ϕ_{PHB}) calculated by $1 − (d_f/D_f)^2$. As the Q_c increased, both the glass transition and the normalized ΔH_r of the PDLLA core slightly increased. Simultaneously, the melting endotherm of the PHB component was reduced, and the apparent crystallinity fraction (ϕ^{DSC}) decreased (Figure 8). The dual melting temperatures of the PHB component also gradually decreased, implying that the PHB lamellae developed in the shell region became thinner. For the core−shell fibers with the lowest PHB content obtained by

Table 2. Flow-Rate Effects of Cone Height, Jet Length, and Thermal Properties of the As-Spun PHB/PDLLA Core/Shell Fibers[a]

Q_c (mL/h)	H_c (mm)	L_j (mm)	ϕ_{PHB} (wt)	$T_{g,PDLLA}$ (°C)	$\Delta H_r/\phi_{PDLLA}$ (J/g)	$T_{m,PHB}$ (°C)	ϕ^{DSC}/ϕ_{PHB}
0.3	1.05	10.7	0.18	57.8	5.59	148.8/167.4	0.48
0.5	1.10	14.0	0.24	58.4	5.59	148.8/168.4	0.54
1.5	1.41	20.4	0.48	59.8	5.53	168.8	0.63
3.0	1.73	22.1	0.68	58.8	4.72	169.2	0.57

[a] ϕ_{PHB} is the weight fraction of PHB component, which is determined from the ratio of $(d_f/D_f)^2$ assuming the densities of PDLLA and PHB are the same at 1.23 g/cm³ [$Q_s = 0.5$ mL/h, 10.5 kV, $H = 28$ cm].
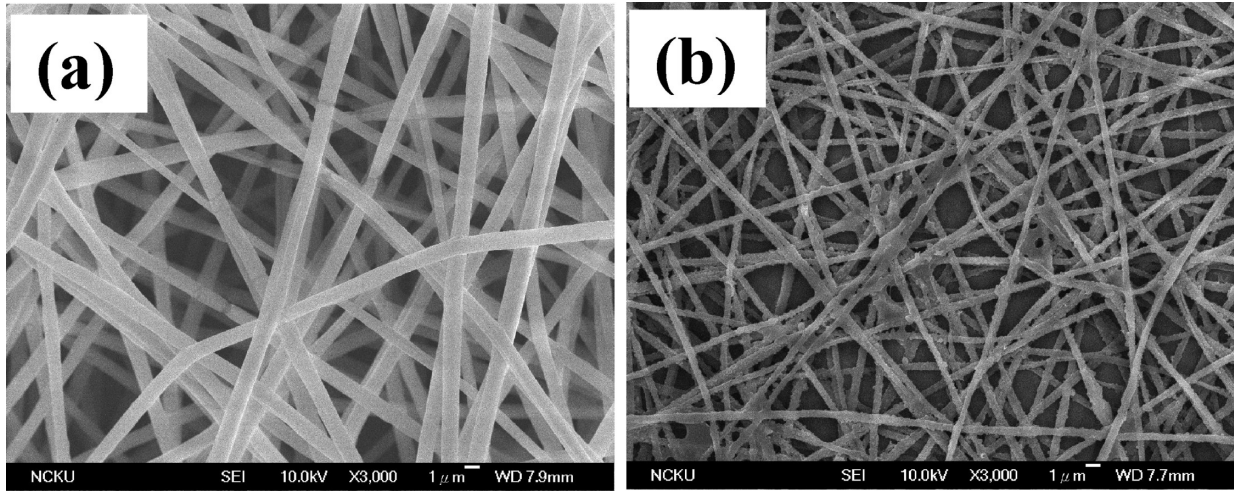

Figure 9. SEM images of PHB/PDLLA core/shell fibers obtained using $Q_c = 0.3$ mL/h: (a) as-spun fibers, (b) fibers after DMF extraction of the outer PDLLA shell [$Q_s = 0.5$ mL/h, 10.5 kV, $H = 28$ cm].

$Q_c = 2.0$ mL/h, a broad melting peak at 166.0 °C and a distinct small endotherm located at 149.4 °C were observed, suggesting the presence of PHB lamellae with two distinct thicknesses. Despite the difference in ϕ^{DSC}, the normalized crystallinity fraction of the PHB component (ϕ^{DSC}/ϕ_{PHB}) was in the range of 0.57−0.65, suggesting that the crystallizability of the PHB chains in the shell part remained relatively unchanged. However, the shell thickness varied from 285 to 120 nm by changing the Q_c from 0.3 to 2.0 mL/h, while the other processing parameters were kept constant.

PHB/PDLLA Core−Shell Fibers. Using the PHB solution as the core fluid and the PDLLA solution as the shell fluid, an alternative form of PHB/PDLLA core−shell fiber was obtained. The processing window was first determined at a given Q_s of 0.5 mL/h (Figure S1). Similarly, with the electrospinning of PDLLA/PHB solutions, both the upper and lower voltages required to develop the cone−jet mode increased with increase in Q_c. On the basis of the processing window, several available Q_c values were selected at a fixed voltage of 10.5 kV to reveal its effect on the cone height, position of the straight jet end, jet diameter, and fiber diameters. The results are tabulated in Table 2. With increasing Q_c, the Taylor cone became bigger, and the straight jet length increased. The former trend was similar, but the latter observation was in striking contrast with the results obtained from electrospinning of the PDLLA/PHB solutions (Figure 2), which exhibited a shorter jet length at a higher Q_c. Figure 9 shows the SEM images of the as-spun core−shell fibers obtained from $Q_c = 0.3$ mL/h as well as those after DMF solvent treatment, which aimed to remove the shell component of PDLLA. In this manner, both values of D_f and d_f were easily determined. As mentioned in the previous section, the d_f value was also estimated by eqs 2 and 3 based on the FTIR result and the flow rate ratio, respectively. The deconvolution of the FTIR spectra in the wavenumber range of 1500−1700 cm⁻¹ was performed, and the results are provided in Figure S2. Figure 10 shows the double-logarithmic plots of D_j, D_f, and d_f versus
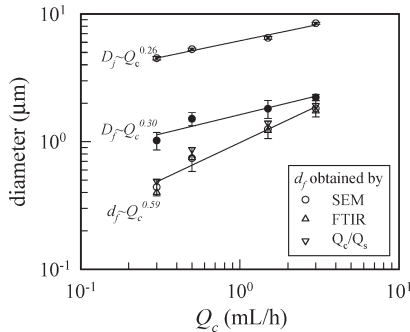

Figure 10. Q_c dependence of the jet diameter (D_j, ⊙), outer fiber diameter (D_f, ●), and inner fiber diameter (d_f: measured by (○) SEM, (△) FTIR, and (▽) flow rates) [$Q_s = 0.5$ mL/h, 10.5 kV, $H = 28$ cm].

Q_c, from which three scaling laws were derived as $D_j \sim Q_c^{0.26}$, $D_f \sim Q_c^{0.30}$, and $d_f \sim Q_c^{0.59}$. Good agreement was achieved for the d_f data obtained from the SEM results, FTIR analysis, and flow-rate calculations. Under the same applied processing variables (i.e., H, Q_s, and V), the measured D_j, d_f, and D_f all increased with the increase in Q_c. Apparently, Q_c showed a less influential effect on the sheath layer than on the fiber outer diameter: as Q_c was increased from 0.3 to 3.0 mL/h, D_f increased from 1.02 to 2.22 μm, but the PDLLA shell thickness exhibited a moderate increase from 0.56 to 0.77 μm.

Given also in Table 2 are the results obtained from the DSC scans of the as-spun PHB/PDLLA core−shell fibers. As the Q_c increased, the PHB content increased. The glass transition of PDLLA was unchanged, but its normalized ΔH_r decreased. The obvious reduction of the normalized crystallinity of the PHB component was observed after applying the lowest Q_c (0.3 mL/h). As shown in Figure S3, the corresponding WAXD profile exhibited only the (020) diffraction plane in the absence of other characteristic planes, indicating that the PHB lamellae

were preferentially oriented with its normal perpendicular to the fiber axis. The cause of this unusual lamellar orientation is currently under investigation. A plausible explanation is the stretching of the core PHB fluid with developing lamellae during jet whipping, which results in the lamellar reorientation.

Flow-Rate Dependence of the Diameters of Jet and Fiber. The exponent for the D_j−Q_c relation (ca. 0.23−0.26) was relatively independent of the interchanging of the core−shell fluids (Figures 6 and 10), but it was smaller than that derived from the single-tube electrospinning (ca. 0.44−0.61).[25,31] A significant difference in the derived exponents for the relations of D_f−Q_c and d_f−Q_c was found by simply interchanging the core−shell fluids. These findings indicate that the jet whipping process (or jet bending instability[3]) plays an important role in the final fiber diameters.

Indeed, the diameter of the electrospun fibers is determined based on the single-tube electrospinning results through the two stretching stages during the process.[25,31] The first stage is jet ejection issued from the apex of the Taylor cone, while a critical voltage is applied. The diameter of the accelerating jet rapidly decreases and reaches a typical value of several micrometers. In this stage, a high draw-down ratio of several hundreds is expected, provided that solvent evaporation is neglected. Because of the excess surface charge and surface perturbation at the straight jet end, jet whipping (or jet bending instability[42,43]) eventually takes place at the straight jet end. This gives rise to the second stage for jet stretching. Owing to the repulsive electric forces acting between the jet segments, the whipping jets are further stretched to become thinner. In the meantime, enhanced solvent evaporation takes place, and the final dried fibers with submicrometer-scaled diameters are collected from the grounded collector. As the electric field for the present electrode configuration is concentrated around the spinneret end, a straight jet with a short length (small L_j) is desirable. Depending on the electric field and solution properties (viscosity is the dominant one), the draw-down ratio resulting from the jet whipping process can be as high as several 10-fold.[25] Because of complex interactions of the processing variables,[43−46] the current research is still far from accurately predicting the final fiber diameter. Empirically, for a given solution, the diameter of the electrospun fiber is quantitatively dependent upon two measured quantities, D_j and L_j. In other words, a straight jet with a smaller D_j and L_j can experience an enhanced electric field for a more effective whipping process, leading to the production of fibers with a lower D_f. For the single-tube process, the jet diameter (D_j) prior to jet whipping has been theoretically derived to be[47]

$$D_j \sim Q_t^{1/2}(\kappa\gamma)^{-1/6} \quad (4)$$

where Q_t is the flow rate of the electrospinning solution. According to eq 4, D_j is strongly correlated with Q_t but is weakly dependent on the solution properties (κ and γ). More importantly, D_j is independent of the solution viscosity, η_0.

Depending on the Q_c/Q_s ratios used for the coaxial electrospinning, the compound jets exhibited different solution properties. When the flow rate of PDLLA solution increased, the compound jet apparently became more conductive and viscous as the values of κ and η_0 were higher for the PDLLA solution than that for the PHB solution. Provided that D_j is plotted against the total flow rate ($Q_t = Q_c + Q_s$), a master curve can be seen in Figure 11 regardless of which solution is selected as the core fluid for the coaxial electrospinning. This derived exponent (∼0.42) was close to that obtained from electrospinning a single-component fluid (∼0.5). Equation 4, derived originally from the
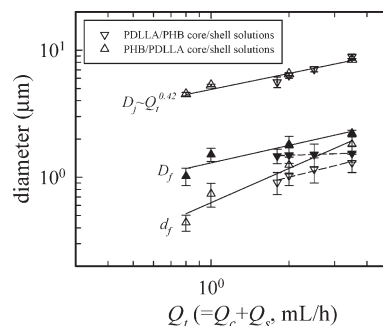

Figure 11. Q_t dependence of the D_j (dotted open symbols), D_f (filled symbols), and d_f (open symbols) for electrospinning the PDLLA/PHB and PHB/PDLLA core/shell solutions. Q_s is fixed at 1.5 and 0.5 mL/h for electrospinning PDLLA/PHB and PHB/PDLLA solutions, respectively. $D_f \sim Q_t^{0.07}$ and $d_f \sim Q_t^{0.51}$ for the PDLLA/PHB solution and $D_f \sim Q_t^{0.46}$ and $d_f \sim Q_t^{0.90}$ for the PHB/PDLLA solution [10.5 kV, $H = 28$ cm].

single-tube process, could be borrowed to predict the Q_t dependence of D_j for coaxial electrospinning. The superposition of the measured data further implied that it was Q_t and not the solution properties that played the key role in determining D_j. Thus, the compound jet can be treated as a single-component fluid flowing from the Taylor cone to the position of L_j.

During the subsequent whipping process, the solution properties of the compound jet began to play an important role as different scaling laws were observed if the inner and outer fluids were exchanged (Figure 11). Previous studies have shown that solutions with a higher conductivity produce an electrified jet with a shorter L_j.[48] As Q_c was increased to electrospin the PDLLA/PHB solutions coaxially, L_j was reduced as the compound jet became more conductive. Therefore, the fatter jet experienced a higher electric strength for jet whipping. This counterbalance eventually gave rise to the weak flow-rate dependence of D_f. For the electrospinning of the PHB/PDLLA core−shell solutions, a larger Q_c led to the formation of less conductive jets, with a larger D_j and a longer L_j, producing fibers with a larger D_f. Our results show that d_f always increases with increasing Q_t (or Q_c), irrespective of the selection of the core fluid, whereas D_f exhibits different levels of Q_t (or Q_c) dependence, depending on the solution properties of the compound jet. Previous reports have shown that Q_s has to be larger than Q_c to obtain a stable cone−jet mode for the production of uniform core−shell fibers.[9,12,49] This is a striking contrast with our present results, which demonstrated that core/shell fibers could be readily obtained using a Q_s/Q_c ratio of 0.75−5.0 to electrospin the PDLLA/PHB solutions and 0.17−1.67 for the PHB/PDLLA solutions.

Drug Release Behavior. Typical electrospun fibers were selected to test their potential application in controlled drug release. They were divided into three groups: the sample codes are shown in Table 3. Samples A and B were single-component fiber mats of PDLLA and PHB, respectively. Samples C, D, and E were the PDLLA/PHB core−shell fiber mats with a difference in DMOG placements (C and D) and shell thickness (D and E). In contrast with samples D and E, interchanging the core−shell fluids led to a production of the PHB/PDLLA core−shell fiber (samples D1 and E1). The cumulative release profiles of the DMOG drug for the fiber mats are shown in Figure 12; the inset is the enlarged portion at a short incubation time. All the samples, except samples D and E, exhibited a one-stage release characteristic, and their release rates depended on the drug placement and fiber diameters. For samples D and E, two-stage release kinetics was observed when DMOG was embedded in the core section: an initial fast release followed by a constant release. In the first stage, the amount released was

Table 3. Different Fibers and Their Corresponding Diameter and Crystallinity Used for Drug Release Experiment

| code	fiber type	Q_c/Q_s (mL/h)	drug in	D_f (μm)	$(D_f - d_f)/2$ (μm)	ϕ_{PHB}	ϕ^{DSC}/ϕ_{PHB}	release type	n	k (d^{-n})
A	PDLLA	2.0	whole	0.36		0.00	amorphous	burst	0.702	59.0
B	PHB	1.5	whole	1.96		1.00	0.61	burst	0.810	34.7
C	PDLLA/PHB	0.5/1.5	shell	1.49	0.23	0.52	0.62	burst	0.784	53.1
D	PDLLA/PHB	0.5/1.5	core	1.49	0.23	0.52	0.62	burst/linear	0.712	13.7
E	PDLLA/PHB	2.0/1.5	core	1.54	0.12	0.29	0.63	burst/linear	0.712	13.7
D1	PHB/PDLLA	1.5/0.5	core	1.81	0.28	0.48	0.63	burst	0.843	24.6
E1	PHB/PDLLA	1.5/2.0	core	1.16	0.29	0.26	0.59	burst	0.772	20.1
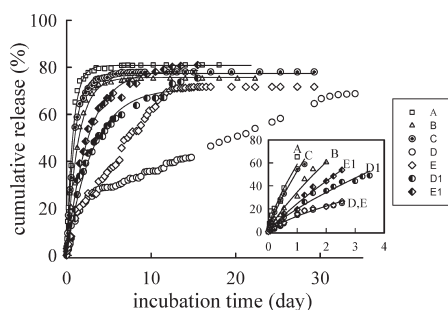
Figure 12. Percentage release of DMOG from electrospun fiber mats versus elapsed time. The inset is the enlarged portion of short releasing time, and the solid lines are the fitting curves by eq 5.

~25% within 60 h, irrespective of the PHB thickness. After the burst release, DMOG was linearly released up to an amount of 70%, and the release rate was relevant with the thickness of the PHB shell. Sample E, with a shell thickness of 120 nm, showed a higher release rate than sample D, with a shell thickness of 230 nm (Table 3). To analyze the release behavior in the initial period quantitatively, the release profiles were fitted with the classical eq 5 to determine the release constant, k.[50,51]

$$M_t/M_\infty = kt^n \qquad (5)$$

where M_t and M_∞ are the amount of drug released at an elapsed time (t) and at saturation, respectively, and n is an exponent dependent on the shape of the release matrix. By plotting $\ln(M_t/M_\infty)$ versus $\ln t$ (Figure S5), the slope and intercept give the values of n and k, respectively. The results are tabulated in Table 3; the solid lines in the inset of Figure 12 show the fitting curves. The derived exponents of n were in the range of 0.70–0.84, suggesting non-Fickian diffusion. The neat PDLLA fiber sample had the largest k value due to the low D_f and its amorphous property. Samples D and E both had a similar first-stage release constant, which possessed the lowest k. As DMOG drugs exhibited better solubility in DMF than in CF, the first-stage release could suggest that some DMOG drugs dissolved in the core PDLLA/DMF fluid could have diffused across the core–shell liquid interface during coaxial electrospinning. In summary, electrospun core–shell fibers provided promising rate-controlled drug release from the matrix, given that the internal structure and diameters of the fibers were suitably adjusted by simply manipulating the flow rate of the core fluid, Q_c.

Conclusion

Electrospun core–shell fibers of PDLLA/PHB and PHB/PDLLA were prepared by a coaxial spinning process. TEM was not a feasible tool in acquiring the core diameter as the electrospun fibers were too thick (shell diameter > 1 μm). After selectively removing the PDLLA component in the as-spun fibers by DMF solvent, the inner and outer diameters of the core–shell fibers were evidently determined by SEM. A consistent core

diameter could also be derived from the solution flow-rate ratio (Q_c/Q_s) and the FTIR spectra of the as-spun fibers based on the assumption that both the core and shell fluids experience the same elongational stretching during the whipping process. This indirect approach provided a convenient estimation of the core diameter without using sophisticated apparatus, such as the fluorescence microscope, which generally requires sensitive dye embedment. Our processing results showed that Q_c was a variable that could be conveniently manipulated to adjust the diameters of the core and shell fibers. Several scaling laws were derived to describe the Q_c dependence of D_j, D_f, and d_f. On the basis of these scaling laws, core–shell fibers with a fixed outer diameter but variable shell thicknesses were prepared for the controlled release of the DMOG drug. When DMOG was loaded in the core section, two-stage release kinetics was observed. A burst release of a small amount of DMOG took place in the first stage, followed by the zero-release order of majority of DMOG in the second stage. As expected, core–shell fibers with a larger shell thickness possessed a lower drug release rate.

Supporting Information Available: Processing window for coaxial electrospinning to prepare the core/shell fibers; FTIR spectra of the as-spun core/shell fibers obtained from electrospinning of solutions with different Q_c; WAXD intensity profiles and DSC heating traces of the as-spun PHB/PDLLA fibers prepared from different Q_c; determination of drug release parameters. This material is available free of charge via the Internet at http://pubs.acs.org.

References and Notes

(1) Greiner, A.; Wendorff, J. H. *Angew. Chem., Int. Ed.* **2007**, *46*, 5670–5703.

(2) Ramakrishna, S.; Kazutoshi, F.; Teo, W.-E.; Lim, T.-C.; Ma, Z. *An Introduction to Nanofibers*; World Scientific: Singapore, 2005.

(3) Reneker, D. H., Fong, H., Eds.; *Polymeric Nanofibers*; ACS Symposium Series 918; American Chemical Society: Washington, DC, 2006.

(4) Reneker, D. H.; Yarin, A. L.; Zussman, E.; Xu, H. *Advances in Applied Mechanics*; Aref, H., Van Der Giessen, E., Eds.; Elsevier/Academic: London, 2007; Vol. *41*, pp 43–195.

(5) Sun, Z.; Zussman, E.; Yarin, A. L.; Wendorff, J. H.; Greiner, A. *Adv. Mater.* **2003**, *15*, 1929–1932.

(6) Loscertales, I. G.; Barrero, A.; Márquez, M.; Spretz, R.; Velarde-Ortiz, R.; Larsen, G. *J. Am. Chem. Soc.* **2004**, *126*, 5376–5377.

(7) Zhang, Y.; Huang, Z. M.; Xu, X.; Lim, C. T.; Ramakrishna, S. *Chem. Mater.* **2004**, *16*, 3406–3409.

(8) Li, D.; McCann, J. T.; Xia, Y. *Small* **2005**, *1*, 83–86.

(9) Wang, M.; Yu, J. H.; Kaplan, D. L.; Rutledge, G. C. *Macromolecules* **2006**, *39*, 1102–1107.

(10) Doro, Y.; Salalha, W.; Avrahami, R.; Zussman, E.; Yarin, A. L.; Dersch, R.; Greiner, A.; Wendorff, J. H. *Small* **2007**, *3*, 1064–1073.

(11) Ojha, S. S.; Stevens, D. R.; Hoffman, T. J.; Stano, K.; Klossner, R.; Scott, M. C.; Krause, W.; Clarke, L. I.; Gorga, R. E. *Biomacromolecules* **2008**, *9*, 2523–2529.

(12) Moghe, A. K.; Gupta, B. S. *Polym. Rev.* **2008**, *48*, 353–377.

(13) Sun, B.; Duan, B.; Yuan, X. *J. Appl. Polym. Sci.* **2006**, *102*, 39–45.

(14) Jiang, H.; Hu, Y.; Li, Y.; Zhao, P.; Zhu, K.; Chen, W. *J. Controlled Release* **2005**, *108*, 237–243.

(15) Chew, S. Y.; Wen, J.; Yim, E. K. F.; Leong, K. W. *Biomacromolecules* **2005**, *6*, 2017–2024.

(16) Huang, Z. M.; He, C. L.; Yang, A.; Zhang, Y.; Han, X. J.; Yin, J.; Wu, Q. *J. Biomed. Mater. Res.* **2006**, *77A*, 169–179.

(17) He, C. L.; Huang, Z. M.; Han, X. J.; Liu, L.; Zhang, H. S.; Chen, L. S. *J. Macromol. Sci., Part B: Phys.* **2006**, *45*, 515–524.

(18) Zhang, Y. Z.; Wang, X.; Feng, Y.; Li, J.; Lim, C. T.; Ramakrishna, S. *Biomacromolecules* **2006**, *7*, 1049–1057.

(19) Xie, J.; Ng, W. J.; Lee, L. Y.; Wang, C. H. *J. Controlled Release* **2008**, *317*, 469–476.

(20) Agarwal, S.; Wendorff, J. H.; Greiner, A. *Polymer* **2008**, *49*, 5603–5621.

(21) McKee, M. G.; Wilkes, G. L.; Colby, R. H.; Long, T. E. *Macromolecules* **2004**, *37*, 1760–1767.

(22) Shenoy, S. L.; Bates, W. D.; Frisch, H. L.; Wnek, G. E. *Polymer* **2005**, *46*, 3372–3384.

(23) Sombatmankhong, K.; Suwantong, O.; Waleetorncheepsawat, S.; Supaphol, P. *J. Polym. Sci., Polym. Phys.* **2006**, *44*, 2923.

(24) Ishii, D.; Lee, W.-K.; Kasuya, K.-I.; Iwata, T. *J. Biotechnol.* **2007**, *132*, 318.

(25) Wang, C.; Hsu, C. H.; Hwang, I. H. *Polymer* **2008**, *49*, 4188–4195.

(26) Agarwal, S.; Wendorff, J. H.; Greiner, A. *Polymer* **2008**, *49*, 5603–5621.

(27) Zong, X.; Kim, K.; Fang, D.; Ran, S.; Hsiao, B. S.; Chu, B. *Polymer* **2002**, *43*, 4403–4412.

(28) Inai, R.; Kotaki, M.; Ramakrishna, S. *Nanotechnology* **2005**, *16*, 208–213.

(29) Bognitzki, M.; Czado, W.; Frese, T.; Schaper, A.; Hellwig, M.; Steinhart, M.; Greiner, A.; Wendorff, J. H. *Adv. Mater.* **2001**, *13*, 70–72.

(30) Kim, K.; Yu, M.; Zong, X.; Chiu, J.; Fang, D.; Seo, Y. S.; Hsiao, B. S.; Chu, B.; Hadjiargyrou, M. *Biomaterials* **2003**, *24*, 4977–4985.

(31) Wang, C.; Chien, H. S.; Yan, K. W.; Hung, C. L.; Hung, K. L.; Tsai, S. J.; Jhang, H. J. *Polymer* **2009**, *50*, 6100–6110.

(32) Bruick, R.; McKnight, S. L. *Science* **2001**, *294*, 1337–1340.

(33) Ivan, M.; Kondo, K.; Yang, H.; et al. *Science* **2001**, *292*, 464–468.

(34) Marchessault, R. H.; Okamura, K.; Su, C. I. *Macromolecules* **1970**, *3*, 735.

(35) Lim, L. T.; Auras, R.; Rubino, M. *Prog. Polym. Sci.* **2008**, *33*, 820.

(36) Barham, P. J.; Keller, A.; Otun, E. L.; Holmes, P. A. *J. Mater. Sci.* **1984**, *19*, 2781.

(37) Similar to the single-component electrospinning reported in ref 38 and coaxial electrospraying reported in ref 39, coaxial electrospinning exhibits different electrospinning modes when the applied voltage is gradually increased provided that Q_c, Q_s, and H are fixed. Staring from the low voltage to the high one, these electrospinning modes can be distinguished: the dripping mode, pulsating mode, cone–jet mode, and unstable mode. The cone–jet mode is the most desirable stage during the electrospinning since a well-controlled process and good reproducibility of fiber properties can be obtained. In other words, there exists a suitable voltage range for coaxial electrospinning. An applied V lower than or higher than this voltage regime will lead to the unstable formation of the Taylor cone. In general, the operating voltage range for the stable cone–jet mode depends on the solution flow rate used. Thus, for a quantitative comparison, the processing window of $V–Q$ should be constructed first in order to select appropriate processing values. The processing windows for the present system are shown in Figure S1 of the Supporting Information.

(38) Shin, Y. M.; Hohman, M. M.; Brenner, M. P.; Rutledge, G. C. *Appl. Phys. Lett.* **2001**, *78*, 1149–1151.

(39) Chen, X.; Jia, L.; Yin, X.; Cheng, J.; Lu, J. *Phys. Fluids* **2005**, *17*, 032101.

(40) Pan, P.; Kai, W.; Zhu, B.; Dong, T.; Inoue, Y. *Macromolecules* **2007**, *40*, 6898–6905.

(41) Yoshie, N.; Oike, Y.; Kasuya, K.; Doi, Y.; Inoue, Y. *Biomacromolecules* **2002**, *3*, 1320–1326.

(42) Shin, Y. M.; Hohman, M. M.; Brenner, M. P.; Rutledge, G. C. *Polymer* **2001**, *42*, 9955.

(43) Reneker, D. H.; Yarin, A. L.; Fong, H.; Koombhongse, S. *J. Appl. Phys.* **2000**, *87*, 4531.

(44) Fridrikh, S. V.; Yu, J. H.; Brenner, M. P.; Rutledge, G. C. *Phys. Rev. Lett.* **2003**, *90*, 144502–1.

(45) Feng, J. J. *J. Non-Newtonian Fluid Mech.* **2003**, *116*, 55.

(46) Helgeson, M. E.; Grammatikos, K. N.; Deitzel, J. M.; Wagner, N. J. *Polymer* **2008**, *49*, 2924.

(47) Gaňán-Calvo, A. M. *Phys. Rev. Lett.* **1997**, *79*, 217.

(48) Wang, C.; Hsu, C. H.; Lin, J. H. *Macromolecules* **2006**, *39*, 7662–7672.

(49) Chakraborty, S.; Liao, I. C.; Adler, A.; Leong, K. W. *Adv. Drug Delivery Rev.* **2009**, *61*, 1043–1054.

(50) Ritger, P. L.; Peppas, N. A. *J. Controled Release* **1987**, *5*, 23–36.

(51) Zeng, J.; Aigner, A.; Czubayko, F.; Kissel, T.; Wendorff, J. H.; Greiner, A. *Biomacromolecules* **2005**, *6*, 1484–1488.